# Fabrication of Au Nanowire/Pichia pastoris Cell Composites with Hexadecyltrimethylammonium Bromides as a Platform for SERS Detection: A Microorganism-Mediated Approach

**ARTICLE** *in* INDUSTRIAL & ENGINEERING CHEMISTRY RESEARCH · DECEMBER 2012

Impact Factor: 2.59 · DOI: 10.1021/ie3026604

I&EC research
Industrial & Engineering Chemistry Research

Article

pubs.acs.org/IECR

# Fabrication of Au Nanowire/*Pichia pastoris* Cell Composites with Hexadecyltrimethylammonium Bromides as a Platform for SERS Detection: A Microorganism-Mediated Approach

Miao Wang, Tao Kong, Xiaolian Jing, Yu-Kao Hung, Daohua Sun, Liqin Lin, Yanmei Zheng, Jiale Huang,* and Qingbiao Li

Department of Chemical and Biochemical Engineering, College of Chemistry and Chemical Engineering, and National Laboratory for Green Chemical Productions of Alcohols, Ethers, and Esters, and Key Lab for Chemical Biology of Fujian Province, Xiamen University, Xiamen, 361005, People's Republic of China

Supporting Information

**ABSTRACT:** Au nanowire/*Pichia pastoris* cell composites were prepared using a microorganism-mediated method, where closely packed Au nanowires (AuNWs) are synthesized at high yields in the presence of hexadecyltrimethylammonium bromide (CTAB) without auxiliary seeds. The initial concentrations of ascorbic acid (AA), CTAB, and tetrachloroaurate trihydrate, as well as the amount of *Pichia pastoris* cells (PPCs), were optimized for the formation of AuNWs. For the formation of AuNWs, Au(III) ions were initially bound by the PPCs and then reduced by AA to produce Au nanoparticles (AuNPs) via preferential nucleation. The linear fusion of these AuNPs influenced by CTAB resulted in the formation of growing AuNWs, whereas the secondary nucleation beyond the PPCs produced small AuNPs that were subsequently consumed through Ostwald ripening during the aging of AuNWs. These AuNW/PPCs composites could be effectively used as surface-enhanced Raman scattering substrates for the detection of rhodamine 6G.

## 1. INTRODUCTION

The synthesis and application of metal nanostructures have attracted increasing attention as advances in nanotechnology in modern science and technology have continued to improve.[1] For example, designing the shape of Au nanostructures has attracted increasing attention because of their intriguing properties and promising applications in nanoelectronics, biomedicine, sensing, and catalysis.[2,3] Au nanostructures such as nanocubes,[4] nanorods,[5−7] nanoplates,[8,9] nanocages,[10] nanowires,[11−20] octahedrons,[21] tetrahedrons,[4] decahedrons,[22] and icosahedrons[23] could be tuned using a variety of chemical, physical, and biological methods. Among these, Au nanowires (AuNWs) are of great interest because of their chemical stability and excellent Au conductivity.[24] Single crystalline,[14−16,19,20] multiple twinned,[12,13] and polycrystalline[20] AuNWs with diameters that range from 2 nm (ultrathin) to hundreds of nanometers could be synthesized through chemical reduction,[13−16] electrochemical,[10,16,19] irradiation,[12] and microwave-assisted[18,19] methods.

Microsized and nanosized templates have also been explored to synthesize and/or immobilize Au nanostructures in a controlled manner to bridge the gap between bulk materials and Au nanostructures for technical applications. Compared with synthetic templates, the use of biotemplates (cell surface layers,[25] viruses,[26] DNA,[27] peptides,[28] proteins,[28] aspartic acid,[29] etc.) can maximize their characteristic nanoscale dimensions, versatility, and specificity.[30,31] Among these biotemplates, crystalline bacterial cell surface layers (S-layers) with a protein superlattice[25,30] have been used for the template-directed assembly of Au nanoparticles (AuNPs) into their superlattice structures.[32−34] However, the tandem shape control and assembly of Au nanostructures over S-layers has not been successfully achieved. Moreover, it requires laborious procedures to isolate S-layers from microorganisms. In this study, we reported that *Pichia pastoris* cells (PPCs) could be directly used instead of S-layers for the surface-mediated growth of closely packed AuNWs in the presence of hexadecyltrimethylammonium bromide (CTAB). In addition, Au nanobelts (AuNBs) and leaflike Au nanostructures were also synthesized by adjusting the CTAB concentration and replacing CTAB with hexadecyltrimethylammonium chloride (CTAC), respectively. AuNWs were interweaved to encapsulate PPCs to form AuNW/PPC composites, which can be directly used as surface-enhanced Raman spectroscopy (SERS) substrates for the detection of rhodamine 6G (R6G). Scanning electron microscopy (SEM), transmission electron microscopy (TEM), selected-area electron diffraction (SAED), and X-ray diffraction (XRD) were performed to characterize Au nanostructures. Fourier transform infrared spectroscopy (FTIR) was performed to investigate the interaction among PPCs, Au(III), and Au nanostructures. Furthermore, the formation mechanism of AuNWs was clarified. Therefore, this study exemplifies the combination of a microorganism and a surfactant for the fabrication of bioorganic−inorganic composite materials as a platform for SERS detection.

**Received:** September 29, 2012
**Revised:** November 29, 2012
**Accepted:** November 30, 2012
**Published:** November 30, 2012





dx.doi.org/10.1021/ie3026604 | *Ind. Eng. Chem. Res.* 2012, 51, 16651−16659

## 2. EXPERIMENTAL SECTION

**2.1. Materials and Chemicals.** Tetrachloroaurate trihydrate ($HAuCl_4 \cdot 3H_2O$, 99.99%) and CTAB (99.9%) were purchased from Sinopharm Chemical Reagent Co., Ltd., China. CTAC (99.9%) and ascorbic acid (AA, 99%) were purchased from Tianjin Guangfu Fine Chemical Research Institute and Sangon Biotech (Shanghai) Co., Ltd., respectively. All chemicals were used without further purification.

**2.2. Cultivation of PPCs and Preparation of Their Powder.** The medium used for growing PPCs contained yeast extract (10 g $L^{-1}$), peptone (20 g $L^{-1}$), and glucose (20 g $L^{-1}$) in deionized water. After the cells were incubated for 48 h at 30 °C and 150 rpm, they were harvested through centrifugation, and then dried in an oven (60 °C) for 24 h. The dried cells were then crushed into fine powders, which were screened through a 100-mesh sieve. The screened cell powder was stored in a desiccator.

**2.3. Synthesis of Au Nanostructures.** For the synthesis of AuNWs, PPCs (0.005−0.01 g) were initially added to aqueous CTAB (10.0 mM). Aqueous $HAuCl_4$ (47 $\mu$L, 0.04856 M) and AA (50 $\mu$L, 0.1 M) were added to produce the initial reaction solutions in flasks with a total volume of 10 mL. The solutions were then agitated (30 °C, 150 rpm) for 1−72 h. The cells interacted with Au(III) for 0−30 min before the AA solution was added. The color of the solutions turned from yellow to colorless immediately after the AA solution was added. Some precipitates were observed at the bottom of the flasks after 1 h. The resulting solutions were sampled and centrifuged at 2000 rpm for 10 min. Thereafter, the supernatant was decanted, and the precipitates were dispersed in 200 $\mu$L of deionized water. For the synthesis of AuNBs, the same procedures for the synthesis of AuNWs were performed, except that a CTAB concentration of 0.005 M was used. For the synthesis of leaflike Au nanostructures, the same procedures for the synthesis of AuNWs were also used, except that CTAB was replaced with CTAC.

**2.4. Characterization of Au Nanostructures.** The TEM samples of AuNWs and AuNBs were prepared by placing a drop of hydrosol on carbon-coated copper grids and allowing water to evaporate completely. TEM observation was performed using a Tecnai F30 Microscope (FEI, The Netherlands). The SEM samples of the suspension were fabricated by dropping the suspension (containing spontaneously formed precipitates) onto clean silicon and allowing water to evaporate completely. SEM observations were carried out using an LEO-1530 electron microscope (LEO, Germany). After the reaction, the resulting solutions were centrifuged at 2000 rpm for 10 min, and the precipitates were dried at 50 °C. The dried mixtures were collected, and an X'Pert Pro X-ray diffractometer (PANalytical BV, The Netherlands) operated at 40 kV and 30 mA with Cu K$\alpha$ radiation was used to determine the formation of Au.

**2.5. Biosorption of Au(III) Ions by PPCs.** The experiments on the biosorption of Au(III) ions by PPCs were conducted in 250 mL Erlenmeyer flasks that contained 100 mL of 1 mM $HAuCl_4$ and 0.4 g of PPCs. The flasks were shaken at 180 rpm in the dark at 30 °C. The samples were obtained at time intervals to measure Au concentration by using an atomic absorption spectrophotometer (Pgeneral, China).

**2.6. FTIR Analysis of PPCs before and after the Reaction.** After the reaction, the residual solution was centrifuged at 4800 rpm for 10 min to obtain the cell residue. The biomass residue was then completely dried at 60 °C. The dried cells before the reaction, the residue of the cells after the reaction, and CTAB were analyzed using an FTIR Nicolet Avatar 330 (Nicolet, USA).

**2.7. Raman Detection of R6G on AuNW/PPC Composites.** After the AuNW/PPC composites were washed with deionized water, 0.005 g of the composites was dried on a glass slide, and 30 $\mu$L ($10^{-6}$ M) of R6G was dropped on the composites for Raman measurement. The Raman spectra were recorded on a Renishaw inVia spectrometer with a 632.8 nm He−Ne laser as the excitation source. The laser power that reached the sample was 0.4 mW. The spectra acquisition time was 10 s, and the spectra were obtained three times.

## 3. RESULTS AND DISCUSSION

**3.1. Synthesis of AuNWs.** *3.1.1. Effect of PPCs.* Well-defined and closely packed AuNWs (Figure 1) could be

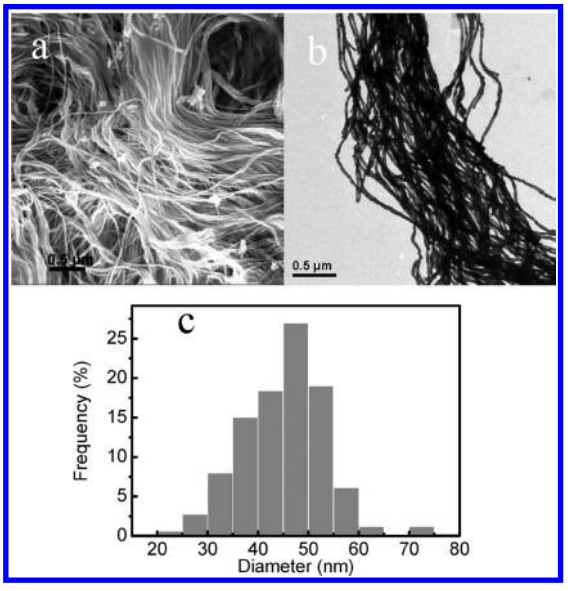


**Figure 1.** (a) SEM image, (b) TEM image, and (c) histogram of the diameter distribution of Au nanowires synthesized through the reduction of aqueous tetrachloroaurate (0.23 mM) with ascorbic acid (0.5 mM) in the presence of PPCs (0.005 g) and hexadecyltrimethylammonium bromide (9.0 mM).

synthesized through the reduction of aqueous $HAuCl_4$ (0.23 mM) with AA (0.5 mM) in the presence of CTAB (9.0 mM) and PPCs (0.005 g) at 30 °C (the center of the schematic coordinate in Scheme 1). Figure 1c shows the histogram of the diameter distribution of AuNWs, which ranged from 20 to 75 nm with a statistical diameter of 45.3 ± 8.6 nm. AuNWs with lengths of >10 $\mu$m were interweaved to encapsulate PPCs to form AuNW/PPC composites with approximately 8.2% Au (mass percentage). The SAED and XRD results confirmed the formation of Au nanostructures. The typical SAED pattern (Figure 2a) from AuNWs revealed Bragg reflections that correspond to {111}, {200}, {220}, and {311}, which indicates that AuNWs were polycrystalline in nature. Jana et al.[5] synthesized Au nanorods in the presence of CTAB by using the seed-mediated growth method in a homogeneous aqueous solution. Furthermore, Kim et al.[13] synthesized twinned AuNWs with a tunable diameter of 20−50 nm instead of Au nanorods with a three-step seed-mediated method by using fewer Au seeds. Ultrathin single crystalline AuNWs were


dx.doi.org/10.1021/ie3026604 | Ind. Eng. Chem. Res. 2012, 51, 16651−16659

**Scheme 1. Synthetic Routes for Au Nanostructures**

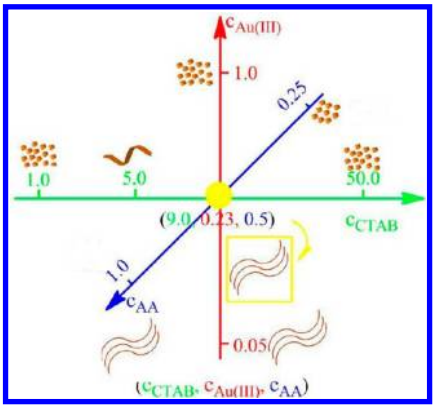


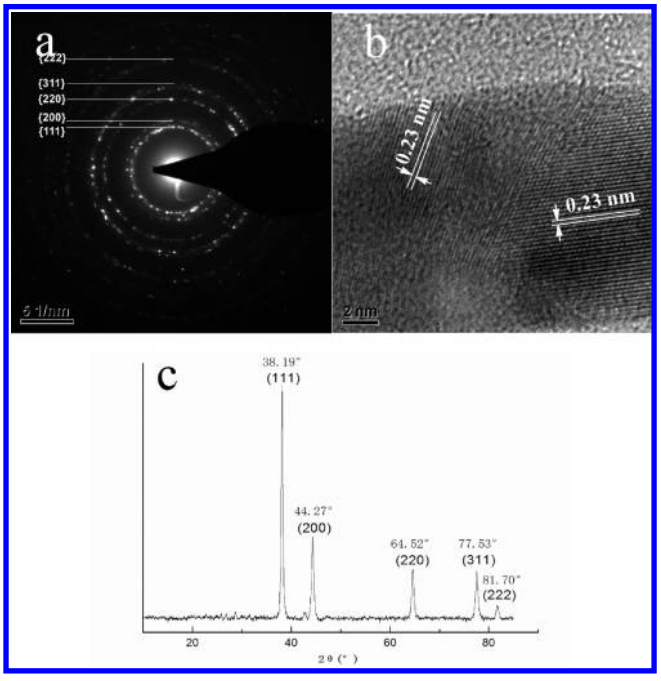


**Figure 2.** (a) Selected-area electron diffraction, (b) high-resolution TEM image, and (c) XRD pattern of Au nanowires synthesized through the reduction of aqueous tetrachloroaurate with ascorbic acid in the presence of hexadecyltrimethylammonium bromide and PPCs at 30 °C.

synthesized in homogeneous organic solutions by three other groups.[14−16] In the current study, AuNWs were easily produced through the synergistic roles of PPCs and CTAB without Au seeds. This study is the first to report on the synthesis of well-defined AuNWs in a heterogeneous solution that contains microbial cells. The polycrystalline AuNWs differed from the twinned and single cystalline ones that were previously synthesized in homogeneous solutions, which could be attributed to the presence of PPCs that can bind Au ions. A couple of Bragg reflections are distinctly exhibited in the XRD pattern of AuNWs (Figure 2c), which may be indexed based on the face-centered-cubic structure of Au. Thus, the XRD pattern clearly shows that AuNWs are essentially crystalline. The high-resolution TEM image of AuNWs (Figure 2b) shows that the crystal plane spacing was approximately 0.23 nm, which corresponds to the Au(111) crystal plane.

The functions of PPCs were preliminarily probed through their absence and presence in the reaction solutions. In the absence of PPCs, chainlike nanostructures (Figure 3a) evolved from the anisotropic growth of AuNPs because of CTAB,

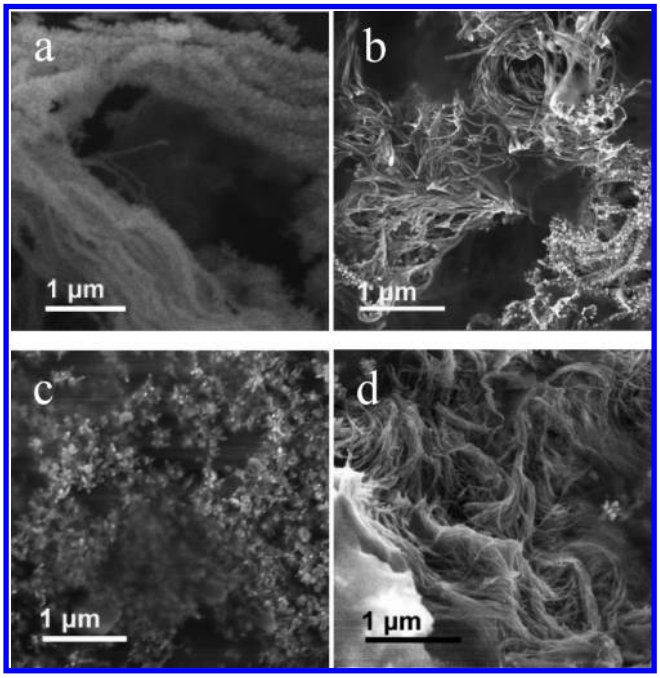


**Figure 3.** SEM images of Au nanostructures synthesized through the reduction of aqueous tetrachloroaurate (0.23 mM) with ascorbic acid (0.5 mM) at 30 °C with hexadecyltrimethylammonium bromide (9.0 mM) (a, top left) in the absence of PPCs and (b−d) in the presence of different amounts of PPCs: (b) 0.01, (c) 0.05, and (d) 0.0025 g.

which is widely used for the synthesis of one-dimensional nanostructures. By contrast, well-defined AuNWs were obtained in the presence of PPCs. The biosorption of Au(III) ions was a rapid process (Figure S1 in Supporting Information). In other words, Au(III) ions can be easily bound by the cells. Therefore, we supposed that the binding sites would become preferential nucleation sites for the growth of AuNPs that would further develop into AuNWs because of CTAB. The adhesion of AuNWs to PPCs was very weak; thus, they could easily fall off the PPCs. Therefore, the as-formed AuNWs did not adhere to PPCs. The effect of the amount of PPCs on the morphology of the Au nanostructures was further investigated to understand the effect of PPCs. By contrast to Figure 1a, the formation of AuNWs and AuNPs in Figure 3b was promoted by doubling the number of cells, whereas only AuNPs were produced by increasing their number by 9-fold (Figure 3c). Thus, more AuNPs were dispersed on the cells by increasing the number of cells. However, AuNPs were less concentrated over PPCs, which prevented the formation of potential AuNWs. Hence, excess amounts of PPCs could form AuNPs rather than AuNWs. However, decreasing the number of cells by half resulted in several AuNWs being severely aggregated (Figure 3d), which may be attributed to the highly concentrated Au ions on PPCs. Therefore, the appropriate amount of PPCs should be determined to form well-defined AuNWs. We tentatively proposed that PPCs have dual functions, i.e., in the biosorption of Au ions and as a platform for preferential nucleation.

*3.1.2. Effect of CTAB.* The morphology of the nanostructures was also affected by the CTAB concentration (green axis of $c_{CTAB}$ in Scheme 1). Aggregates of AuNPs instead of AuNWs


dx.doi.org/10.1021/ie3026604 | *Ind. Eng. Chem. Res.* 2012, 51, 16651−16659

were formed without CTAB (Figure S2 in the Supporting Information). An accurate CTAB concentration (0.009 M) was essential for the production of AuNWs (Figure 1a). Figure 4

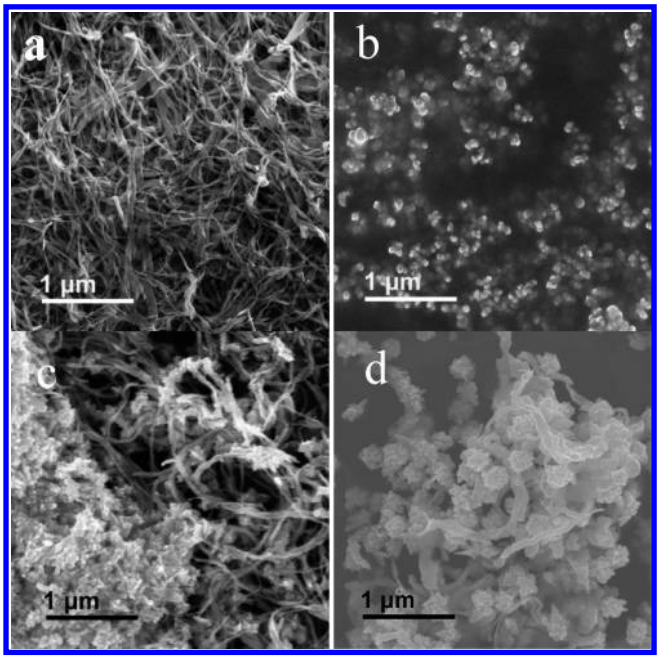


**Figure 4.** SEM images of Au nanostructures synthesized through the reduction of aqueous tetrachloroaurate (0.23 mM) with ascorbic acid (0.5 mM) at 30 °C in the presence of the PPCs (0.005 g) in different hexadecyltrimethylammonium bromide concentrations: (a) 0.005, (b) 0.001, (c) 0.05, and (d) 0.1 M.

shows the SEM images of Au nanostructures produced at different CTAB concentrations. AuNBs (Figure 4a), rather than AuNWs, were produced when the CTAB concentration was decreased to 0.005 M. However, only aggregations of small AuNPs (Figure 4b) were observed when the concentration was further decreased to 0.001 M. Moreover, the percentage of AuNWs decreased and AuNPs were promoted (Figure 4c and 4d, respectively) by increasing the CTAB concentration to 0.05 and 0.1 M, respectively. The function of CTAB in the seeding growth of Au nanorods (AuNRs) remains controversial. CTAB has been known to form micelles to induce and direct one-dimensional growth.[1] Conversely, Garg et al.[35] demonstrated that $Br^-$ functions as an important shape-directing agent in the formation of AuNRs in the seed-mediated process. In the present study, $Br^-$ also promoted the formation of AuNWs without seeds; thus, AuNWs could not be obtained when CTAB was replaced with CTAC at an equal concentration (Figure 5). The remarkable difference between CTAB and CTAC was that $Br^-$ was more easily adsorbed on the crystal facet than $Cl^-$; thus, $Cl^-$ had a slight effect on the formation of nanostructures.[35] Leaflike Au nanostructures with a two-dimensional orientation were produced in the presence of CTAC. The results indicate to some extent that $CTA^+$ ions can promote the anisotropic growth of Au nanostructures. Hence, the shape-directing role of $CTA^+$ could not be neglected even if $Br^-$ has an important function in the formation of AuNWs. When the $CTA^+$ concentration was low, the Au particles grew anisotropically as $CTA^+$ was selectively adsorbed onto several specific crystal facets to enable preferential growth of other facets. The resulting anisotropic particles tended to connect together to form AuNWs because of the effect of $Br^-$.

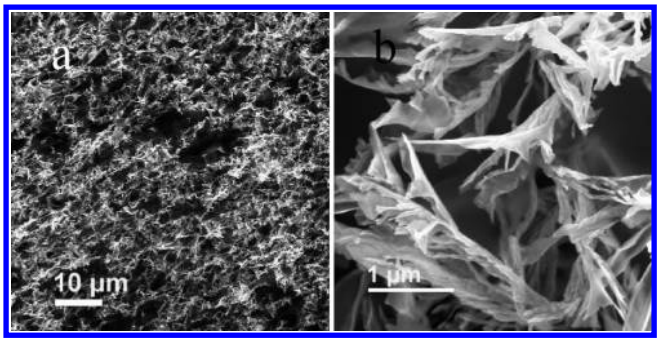


**Figure 5.** SEM images of Au nanostructures synthesized through the reduction of aqueous tetrachloroaurate (0.23 mM) with ascorbic acid (0.5 mM) at 30 °C in the presence of PPCs (0.005 g) and hexadecyltrimethylammonium chloride (0.009 M).

Therefore, AuNBs can be formed by merging several short AuNWs with poorly protected crystal facets at a lower CTAB concentration. The marked shift from one-dimensional AuNWs to two-dimensional leaflike nanostructures indicated that insufficient $Br^-$ was responsible for the formation of AuNBs, which exhibited both one-dimensional and two-dimensional features. Moreover, the $Br^-$ concentration was very low to promote the formation of AuNWs at very low CTAB concentrations. However, the percentage of AuNWs decreased and AuNPs were promoted at a higher CTAB concentration because of the stronger protection from $CTA^+$. At high $CTA^+$ concentrations, different crystal facets of Au nuclei that were uniformly capped with $CTA^+$ exhibited the same growth rate, which led to the isotropic growth of Au particles. In the absence of CTAB, more Au ions were bound by PPCs. The reduction with AA allowed the nucleation to occur on PPCs, thereby forming AuNPs on the cells. Nevertheless, these AuNPs were easily stripped off the PPCs and aggregated with one another because CTAB was insufficient. Aside from the appropriate CTAB concentration, these AuNPs that formed on PPCs were essential for the growth of AuNWs, which will be discussed in detail in section 3.2.

*3.1.3. Effect of AA.* The reductant AA had an important function in kinetically controlling the Au nanostructures. By contrast to the closely packed AuNWs (Figure 1a) synthesized at 0.5 M AA (blue axis in Scheme 1), only short AuNRs and AuNPs (Figure 6a) were obtained by reducing by half the optimum AA concentration for AuNWs. Conversely, when the

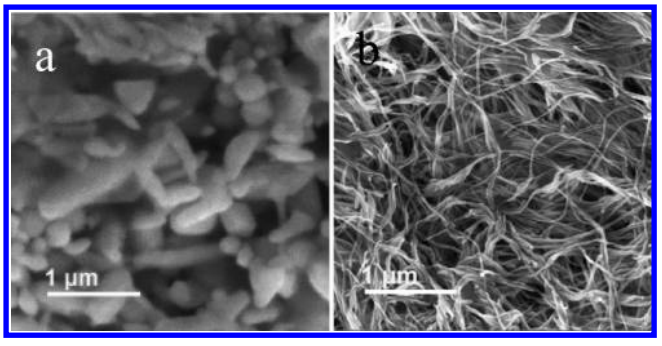


**Figure 6.** SEM images of Au nanostructures synthesized through the reduction of aqueous tetrachloroaurate (0.23 mM) at different concentrations of ascorbic acid, (a) 0.25 and (b) 1.0 mM, in the presence of PPCs (0.005 g) and hexadecyltrimethylammonium bromide (9.0 mM) at 30 °C.


dx.doi.org/10.1021/ie3026604 | *Ind. Eng. Chem. Res.* 2012, 51, 16651−16659

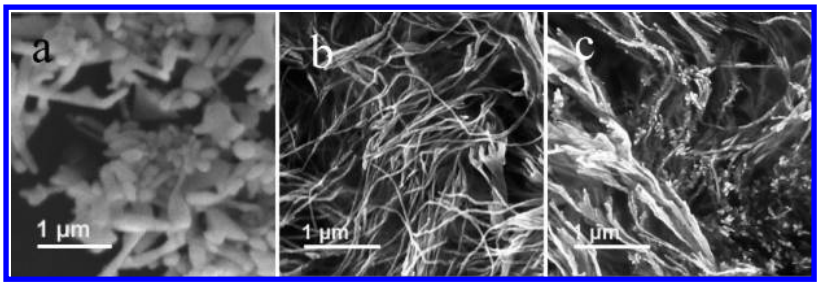


**Figure 7.** SEM images of Au nanostructures synthesized through the reduction of aqueous tetrachloroaurate at (a) 0.5, (b) 0.125, and (c) 0.05 mM with ascorbic acid (0.5 mM) and hexadecyltrimethylammonium bromide (9.0 mM) in the presence of PPCs (0.005 g) at 30 °C.

AA concentration was doubled, a few rough AuNWs were obtained (Figure 6b). At an $HAuCl_4$ concentration of 0.23 mM, 0.69 mM $e^-$ is needed for the complete reduction of Au(III) to Au(0). For the well-defined AuNWs, 0.5 mM AA could provide 1.0 mM $e^-$,[36] which indicates that AA was present in excessive amounts. Furthermore, doubling the AA concentration (i.e., 1.0 mM AA) increased the production rate of the Au atoms. The one-dimensional growth of Au nanostructures was rapidly promoted by CTAB. As a result, a few branched AuNWs were produced (Figure 6b). On the contrary, a low AA concentration (0.25 mM) was insufficient to reduce all Au(III) to Au (0). Therefore, sufficient Au atoms could not be produced in a short time to facilitate the formation of AuNWs. Instead, numerous polydispersed AuNPs were produced (Figure 6a). Thus, excess amounts of AA are necessary to form well-defined AuNWs.

*3.1.4. Effect of $HAuCl_4$.* $HAuCl_4$ concentration (red axis of $c_{Au(III)}$ in Scheme 1) was another factor that affected the morphology of the as-synthesized Au nanostructures. In the presence of CTAB, large AuNPs and AuNRs (Figure 7a) were obtained when a higher $HAuCl_4$ concentration (0.5 mM) was used. AuNWs (Figure 7b) that are similar to those in Figure 1a could also be produced at a lower $HAuCl_4$ concentration (0.125 mM). However, decreasing the $HAuCl_4$ concentration produced numerous AuNPs and branched AuNWs (Figure 7c). At an $HAuCl_4$ concentration of 0.5 M, 1.5 mM $e^-$ was needed to complete the reduction of Au(III) to Au(0). However, 0.5 mM AA could only produce 1 mM $e^-$,[36] which led to the slow growth of Au nanostructures. Simultaneously, CTAB was insufficient for the one-dimensional growth of Au nanostructures. Thus, only some AuNPs and AuNRs were obtained. AuNWs could still be obtained (Figure 7b) by decreasing the $HAuCl_4$ concentration by half, whereas further reducing the $HAuCl_4$ concentration produced several AuNPs (Figure 7c) mainly because of the strong protection of excess amounts of CTAB compared with that of $HAuCl_4$.

**3.2. Formation Mechanism of AuNWs.** We wanted to understand the formation mechanism of AuNWs. The interactions between PPCs and Au(III) ions should be clarified. Figure 8 shows the FTIR spectra of CTAB (curve I) and PPCs (curve II), where both curves were used as the control samples. The FTIR spectra of PPCs after they interacted with Au(III) for 5 min in the absence (curve III) and presence (curve IV) of CTAB are also shown. Figure 8 also shows PPCs after they interacted with Au(III) in the presence of CTAB for 20 (curve V) and 30 min (curve VI). Previous studies have reported that Au(III) was bound by oxygenous- and nitrogenous-active groups of polysaccharides and proteins in the cell wall biopolymers, such as the hydroxyl group of the saccharides, the carboxylate anion of amino acid residues (side chains of the polypeptide backbone), and peptide bond (amide I and amide II bands), among others.[37] By comparing curve II with curves III, IV, V, and VI, the same absorption band at 1074 $cm^{-1}$ that corresponds to a coupled vibration, which involves C−O stretching and O−H deformation modes ($\upsilon_{C-O} + \delta_{O-H}$) of the free hydroxyl group (−C−O−H) of the saccharides,[37] was found. This result indicates that Au(III) ions were not bound by the saccharides. The adsorption of Au(III) on PPCs induced a remarkable red shift of the absorption from 1402 (curve II) to 1383 $cm^{-1}$ (curves III, IV, V, and VI), which could be attributed to the chelation of Au(III) with oxygen in the carboxylate anion.[37] The adsorption at 1549 $cm^{-1}$ (curve II) resulted from a coupled vibration that involves C−N stretching and N−H bending modes ($\upsilon_{C-N} + \delta_{N-H}$) of C−N−H group from the peptide bond (−HN—C═O), i.e., from the amide II band.[37] Thus, a red shift from 1549 $cm^{-1}$ (curve II) to 1545 or 1544 $cm^{-1}$ (curves III, IV, V, and VI) resulted after the PPCs were in contact with Au(III), which was attributed to Au(III) binding of nitrogen in the amide II band.[37] Finally, a blue shift (high-frequency shift) was observed from 1639 (curve IV) to 1641 $cm^{-1}$ (curve V), and then to 1645 $cm^{-1}$ (curve VI), which can be attributed to the gradual complexation of Au(III) with the oxygen in the carbonyl group (C═O) in the peptide bond, i.e., of the amide I band.[37] In summary, Au(III) interacted with oxygenous- and nitrogenous-active groups in the carboxylate anion of amino acid residues (side chains of the polypeptide backbone) and peptide bond (amide I and II bands). Moreover, the similarity of curves IV, V, and VI to curve III as well as the difference between curves IV, V, and VI and curve I clearly shows that the interaction between Au ions and PPCs in the presence of CTAB is similar to that in the absence of CTAB. The presence of CTAB had a slight influence on their interaction. However, only some Au(III) ions were adsorbed onto the PPCs because the amount of Au precursor was much higher than the maximum uptake of Au(III) by PPCs; therefore, the secondary nucleation in the solution was promoted.

Based on the interaction between Au(III) and PPCs above, the growth mechanism of AuNHs could be clarified by sampling the nanostructures at different reaction times for TEM observations. After the addition of $HAuCl_4$, the mixture of PPCs, CTAB, and $[AuCl_4]^-$ turned yellow at the beginning of the reaction because of the presence of ligand-substituted anions such as $[AuCl_3Br]^-$ or CTAB−Au(III) complexes, or both.[38] However, the color of the solution changed from yellow to pale yellow after 30 min of adsorption because the part of the ligand-substituted anions was broken. This break is due to adsorption of Au(III) on the PPCs, which is shown in the FTIR spectra (Figure 8). Thirty minutes of adsorption gave rise to a saturated adsorption and adsorbed Au(I) ions[36] which stemmed from bioreduction of Au(III). Therefore, they were

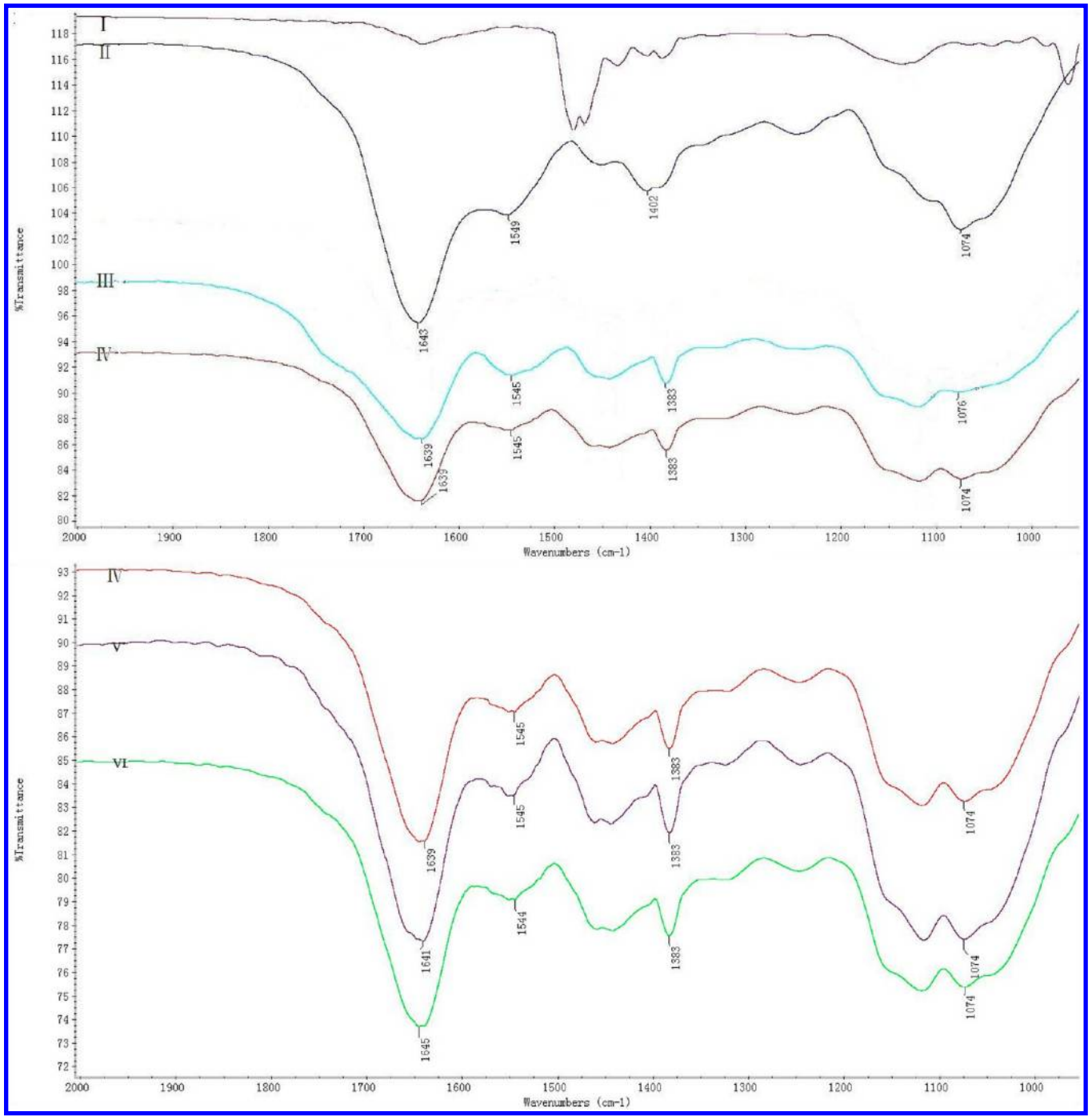


**Figure 8.** FTIR spectra of (I) CTAB, (II) PPCs, (III) PPCs after interacting with Au(III) for 5 min in the absence of CTAB, (IV) PPCs after interacting with Au(III) for 5 min in the presence of CTAB, (V) PPCs after interacting with Au(III) for 20 min in the presence of CTAB, and (VI) PPCs after interacting with Au(III) for 30 min in the presence of CTAB, respectively.

more easily to be totally reduced to Au(0) by AA than Au(III) free in solution. Besides, PPCs could serve as nucleation sites. Therefore, the crystal nucleus could be formed on the PPCs preferentially after addition of AA. Upon addition of AA, the color of the solution immediately changed from pale yellow to colorless, which suggests that Au(III) ions were initially reduced to aqueous Au(I) anions such as $[AuCl_2]^-$ rather than Au(0).[38] Therefore, it could be supposed that most Au(I) ions were present in solution even after the Au nucleus on PPCs had been formed. In the formation of crystal nucleus, the $CTA^+$ adsorbing on the crystal nucleus made the nanostructure electropositive. According to electrostatic interaction, $[AuCl_2]^-$ ions in solution could be attracted to the crystal nucleus and be further reduced to Au(0), which contributed to the growth of AuNPs on PPCs (Figure 9a,b). To some extent, the role of the crystal nucleus on PPCs is similar to the Au seed in the traditional seed-mediated method for the preparation of Au nanorods, which could be used to prepare considerably homogeneous Au nanorods. Therefore, compared to the heterogeneous nanostructures formed without PPCs (Figure 3a), the formation of AuNPs was much more homogeneous in the presence of PPCs. These preferential nucleation sites


dx.doi.org/10.1021/ie3026604 | *Ind. Eng. Chem. Res.* 2012, 51, 16651−16659

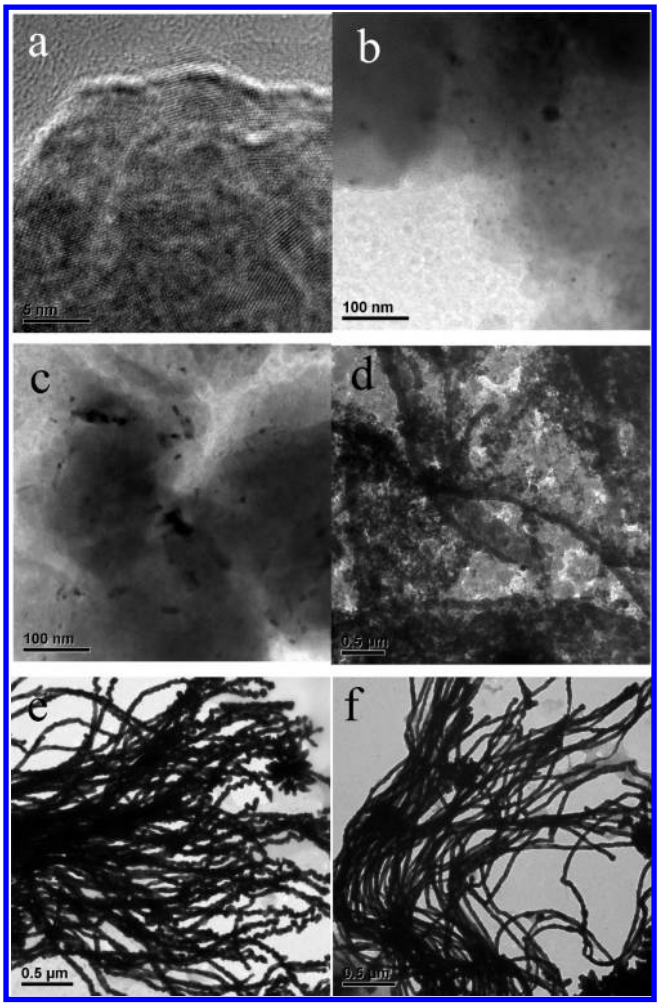


**Figure 9.** Au nanostructures synthesized through the reduction of aqueous tetrachloroaurate (0.23 mM) with ascorbic acid (0.5 mM) for (a) 1, (b) 1, (c) 2, (d) 5, (e) 10, and (f) 120 min in the presence of PPCs (0.005 g) and hexadecyltrimethylammonium bromide (9.0 mM).

rapidly concentrated Au atoms and experienced anisotropic growth into some nanorods on PPCs in the presence of CTAB (Figure 9c). AuNPs that formed on PPCs underwent further linear fusion into AuNWs under the direction of $Br^-$ (Figure 9d), which demonstrated the supposition that the PPCs work as platforms for the formation of initial AuNWs (the effect of PPCs). As the reduction reaction continued, the further growth of the growing AuNWs resulted in chainlike nanostructures (Figure 9e), which was induced by CTAB as discussed in section 3.1.2. The formed AuNWs were easily released into the solution because of the weak interaction between them and PPCs. The reduction of Au(III) in the solution (beyond PPCs) allowed secondary nucleation to occur, which produced AuNPs that would be consumed later through Ostwald ripening during the growth of AuNWs. After 2 h, most chainlike nanostructures evolved to form smooth AuNWs through Ostwald ripening where small AuNPs that stemmed from the secondary nucleation in the solution were consumed (Figure 9f).

Based on the TEM images, we proposed a schematic diagram of the formation of AuNW/PPC nanocomposites. First, the interaction between PPCs and $[AuCl_4]^-$ for more than 30 min allowed some Au(III) ions to be adsorbed onto PPCs (stage I), whereas the others formed ligand-substituted anions with CTAB (Figure 10). After the addition of surplus AA, the reduction of the adsorbed Au(III) ions on PPCs formed Au nuclei that functioned as the preferential nucleation sites for the formation of AuNPs (stage II). The linear fusion of these AuNPs produced chainlike Au nanostructures when they were induced by CTAB (stage III). Simultaneously, the reduction of Au(III) in the solution (beyond PPCs) caused secondary nucleation to occur, thereby producing AuNPs that would be consumed later through Ostwald ripening during the growth of AuNWs. Thus, well-defined AuNWs were formed through Ostwald ripening with AuNPs in the solution (stage IV).

**3.3. Applications of AuNWs.** Au nanostructures have been widely used as SERS substrates because of their strong enhancement of the Raman signal. Previous studies have shown that small AuNP dimers and aggregates, wherein the interstitial sites are the superenhancing location that produce the "hot spot" for the enhancement of Raman signals, have excellent efficiency for SERS.[39] In our SERS experiment, R6G was chosen as the molecule probe because it has been widely used for SERS studies because of its large scattering cross section. AuNPs that were produced using the same method for AuNWs were used as the control samples. The Raman spectra of R6G on AuNPs and AuNWs are shown in Figure 11. AuNWs show a stronger enhancement than AuNPs, which exhibited a weak enhancement. Accordingly, the bands at 615, 773, and 1309 $cm^{-1}$ were attributed to the in-plane deformation vibration of the ring, in-plane stretching vibration of C−H, and in-plane stretching vibration of N−H, respectively. All the bands at 1362, 1507, 1573, and 1648 $cm^{-1}$ were attributed to C−C stretching vibration of the ring. These results are in agreement with the data in a previous report.[40] Unlike AuNPs, the closely packed AuNWs grew into bundles and might form hot spots between them, which trapped the analyst to generate high Raman enhancement. By contrast to most previous studies on the application of Au nanostructures to SERS,[41] the SERS enhancement in the present study was attributed to AuNW/PPC composites, where PPCs were surrounded by closely packed AuNWs. Separating the PPCs from AuNWs was not necessary; however, the presence of PPCs greatly lowered the amount of Au and enabled easier SERS detection.

## 4. CONCLUSIONS

In summary, we developed a seedless and microorganism-mediated method to synthesize closely packed and long AuNWs in the presence of PPCs and CTAB. PPCs possessed dual functions, i.e., in the biosorption of Au ions and as a platform for preferential nucleation for the formation of long and smooth AuNWs. Furthermore, adequate CTAB concentration was needed since both the one-dimensional direction effect of $Br^-$ and anisotropic growth of AuNPs favored by $CTA^+$ were important for the anisotropic growth into AuNWs. For the kinetic factors, an excessive amount of AA was necessary for the kinetic formation of AuNWs. As far as the growth mechanism of AuNWs was concerned, Au ions were initially adsorbed by PPCs and then reduced to form AuNPs on PPCs. These AuNPs experienced an anisotropic growth because of the influence of CTAB to form the growing AuNWs. Then, the secondary nucleation in the solution produced small AuNPs that were subsequently consumed through Ostwald ripening during the growth of AuNWs. Interestingly, the AuNW/PPC nanocomposites in which the

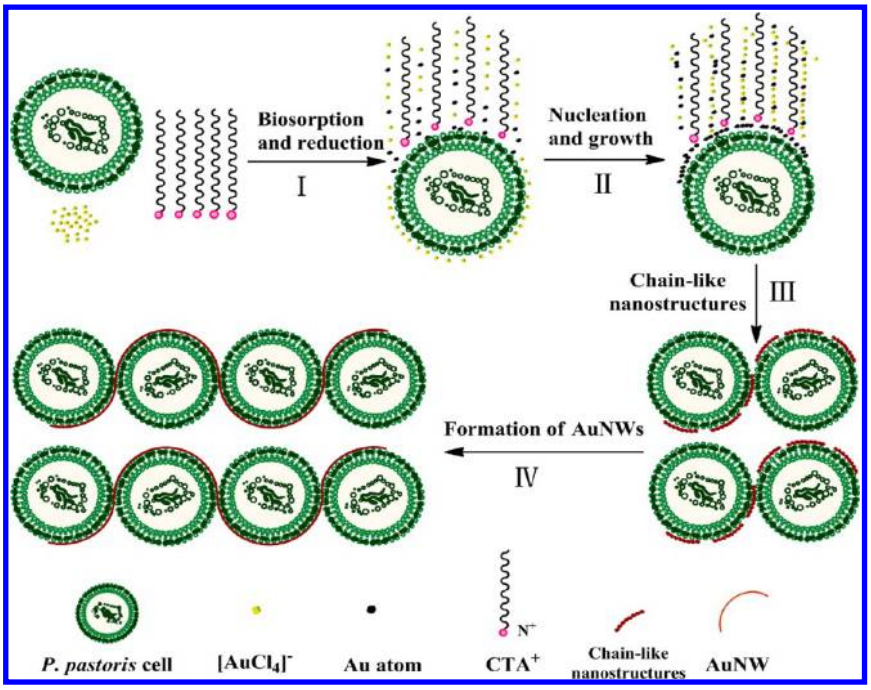


**Figure 10.** Schematic diagram of the formation of AuNW/PPC nanocomposites through the reduction of aqueous tetrachloroaurate with ascorbic acid in the presence of PPCs and hexadecyltrimethylammonium bromide.

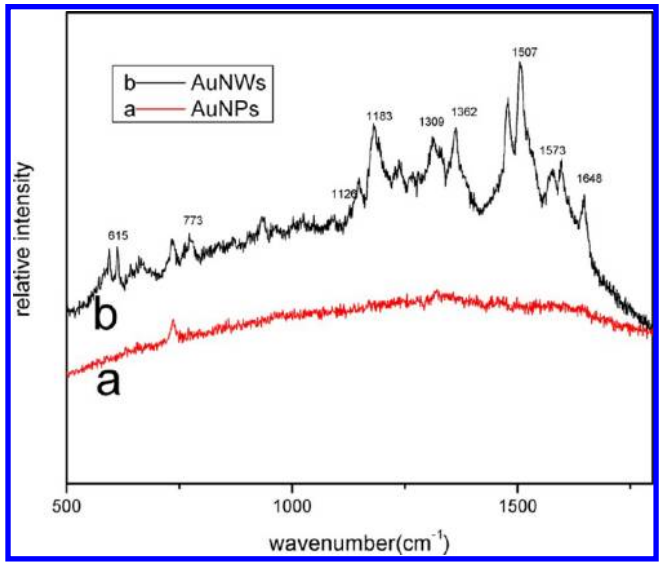


**Figure 11.** Raman spectra of (a) Au nanoparticles and (b) Au nanowires adsorbed with rhodamine 6G ($10^{-6}$ M).

AuNWs showed excellent SERS enhancement can be directly used as SERS substrates.

## ■ ASSOCIATED CONTENT

### Supporting Information

Figure S1 showing percentages of Au adsorbed by PPCs as a function of time and Figure S2 showing SEM images of Au nanostructures. This material is available free of charge via the Internet at http://pubs.acs.org.

## ■ AUTHOR INFORMATION

### Corresponding Author

*E-mail: cola@xmu.edu.cn. Tel.: (+86) 592-2183088. Fax: (+86) 592-2184822.

### Notes

The authors declare no competing financial interest.

## ■ ACKNOWLEDGMENTS

This work was supported by the Fundamental Research Funds for Central Universities (Grant 2010121051), the NSFC projects (Grants 21106117, 21036004, and 20976146), the Research Fund for the Doctoral Program of Higher Education of China (Grants 20100121110032 and 20110121120018), and the NSF-Fujian projects (Grant 2010J05032). The authors extend their gratitude to Prof. Zhongyu Lin, Prof. Guobin Han, and Prof. Jian Weng for their help. Y.-K.H. also expresses gratitude to Xiamen University for an internship.

## ■ REFERENCES

(1) Xia, Y.; Xiong, Y. J.; Lim, B.; Skrabalak, S. E. Shape-controlled synthesis of metal nanocrystals: simple chemistry meets complex physics? *Angew. Chem., Int. Ed.* **2009**, *48*, 60.

(2) Cobley, C. M.; Chen, J. Y.; Cho, E. C.; Wang, L. V.; Xia, Y. N. Gold nanostructures: a class of multifunctional materials for biomedical applications. *Chem. Soc. Rev.* **2011**, *40*, 44.

(3) Takezaki, M.; Aoki, H.; Kodama, M.; Tominaga, T. Interactions between $AuCl_4^-$ and $CTA^+$ ions in water. Enthalpies for the formation of the precipitate. *J. Therm. Anal. Calorim.* **2010**, *101*, 1149.

(4) Kim, F.; Connor, S.; Song, H.; Kuykendall, T.; Yang, P. D. Platonic gold nanocrystals. *Angew. Chem., Int. Ed.* **2004**, *43*, 3673.

(5) Jana, N. R.; Gearheart, L.; Murphy, C. J. Wet chemical synthesis of high aspect ratio cylindrical gold nanorods. *J. Phys. Chem. B* **2001**, *105*, 4065.

(6) Busbee, B. D.; Obare, S. O.; Murphy, C. J. An improved synthesis of high-aspect-ratio gold nanorods. *Adv. Mater.* **2003**, *15*, 414.

(7) Yang, D. P.; Cui, D. X. Advances and Prospects of Gold Nanorods. *Chem.—Asian J.* **2008**, *3*, 2010.

(8) Shankar, S. S.; Rai, A.; Ankamwar, B.; Singh, A.; Ahmad, A.; Sastry, M. Biological synthesis of triangular gold nanoprisms. *Nat. Mater.* **2004**, *3*, 482.

(9) Huang, J. L.; Wang, W. T.; Lin, L. Q.; Li, Q. B.; Lin, W. S.; Li, M.; Mann, S. A general strategy for the biosynthesis of gold nanoparticles

by traditional Chinese medicines and their potential application as catalysts. *Chem.—Asian J.* **2009**, *4*, 1050.
(10) Xia, Y. N.; Skrabalak, S. E.; Chen, J. Y.; Sun, Y. G.; Lu, X. M.; Au, L.; Cobley, C. M. Gold nanocages: synthesis, properties, and applications. *Acc. Chem. Res.* **2008**, *41*, 1587.
(11) Ji, C. X.; Searson, P. C. Synthesis and characterization of nanoporous gold nanowires. *J. Phys. Chem. B* **2003**, *107*, 4494.
(12) Kim, J. U.; Cha, S. H.; Shin, K.; Jho, J. Y.; Lee, J. C. Preparation of gold nanowires and nanosheets in bulk block copolymer phases under mild conditions. *Adv. Mater.* **2004**, *16*, 459.
(13) Kim, F.; Sohn, K.; Wu, J. S.; Huang, J. X. Chemical synthesis of gold nanowires in acidic solutions. *J. Am. Chem. Soc.* **2008**, *130*, 14442.
(14) Huo, Z. Y.; Tsung, C. K.; Huang, W. Y.; Zhang, X. F.; Yang, P. D. Sub-two nanometer single crystal Au nanowires. *Nano Lett.* **2008**, *8*, 2041.
(15) Lu, X. M.; Yavuz, M. S.; Tuan, H. Y.; Korgel, B. A.; Xia, Y. N. Ultrathin gold nanowires can be obtained by reducing polymeric strands of oleylamine-AuCl complexes formed via aurophilic interaction. *J. Am. Chem. Soc.* **2008**, *130*, 8900.
(16) Wang, C.; Hu, Y. J.; Lieber, C. M.; Sun, S. H. Ultrathin Au nanowires and their transport properties. *J. Am. Chem. Soc.* **2008**, *130*, 8902.
(17) Zhang, X. Y.; Li, D.; Bourgeois, L.; Wang, H. T.; Webley, P. A. Direct electrodeposition of porous gold nanowire arrays for biosensing applications. *ChemPhysChem* **2009**, *10*, 436.
(18) Kundu, S.; Liang, H. Microwave synthesis of electrically conductive gold nanowires on DNA scaffolds. *Langmuir* **2008**, *24*, 9668.
(19) Tsuji, M.; Hashimoto, M.; Nishizawa, Y.; Tsuji, T. Synthesis of gold nanorods and nanowires by a microwave-polyol method. *Mater. Lett.* **2004**, *58*, 2326.
(20) Liu, J.; Duan, J. L.; Toimil-Molares, E.; Karim, S.; Cornelius, T. W.; Dobrev, D.; Yao, H. J.; Sun, Y. M.; Hou, M. D.; Mo, D.; Wang, Z. G.; Neumann, R. Electrochemical fabrication of single-crystalline and polycrystalline Au nanowires: the influence of deposition parameters. *Nanotechnology* **2006**, *17*, 1922.
(21) Li, C. C.; Shuford, K. L.; Park, Q. H.; Cai, W. P.; Li, Y.; Lee, E. J.; Cho, S. O. High-yield synthesis of single-crystalline gold nano-octahedra. *Angew. Chem., Int. Ed.* **2007**, *46*, 3264.
(22) Koga, K.; Ikeshoji, T.; Sugawara, K. Size- and temperature-dependent structural transitions in gold nanoparticles. *Phys. Rev. Lett.* **2004**, *92*, No. 115507.
(23) Xu, J.; Li, S. Y.; Weng, J.; Wang, X. F.; Zhou, Z. M.; Yang, K.; Litt, M.; Chen, X.; Cui, Q.; Cao, M. Y.; Zhang, Q. Q. Hydrothermal syntheses of gold nanocrystals: From icosahedral to its truncated form. *Adv. Funct. Mater.* **2008**, *18*, 277.
(24) Wang, C.; Sun, S. H. Facile synthesis of ultrathin and single-crystalline Au nanowires. *Chem.—Asian J.* **2009**, *4*, 1028.
(25) Sleytr, U. B.; Messner, P.; Pum, D.; Sara, M. Crystalline bacterial cell surface layers (S layers): From supramolecular cell structure to biomimetics and nanotechnology. *Angew. Chem., Int. Ed.* **1999**, *38*, 1035.
(26) Dujardin, E.; Peet, C.; Stubbs, G.; Culver, J. N.; Mann, S. Organization of metallic nanoparticles using tobacco mosaic virus templates. *Nano Lett.* **2003**, *3*, 413.
(27) He, Y.; Ye, T.; Ribbe, A. E.; Mao, C. D. DNA-templated fabrication of two-dimensional metallic nanostructures by thermal evaporation coating. *J. Am. Chem. Soc.* **2011**, *133*, 1742.
(28) Dickerson, M. B.; Sandhage, K. H.; Naik, R. R. Protein- and peptide-directed syntheses of inorganic materials. *Chem. Rev.* **2008**, *108*, 4935.
(29) Tan, Y. N.; Lee, J. Y.; Wang, D. I. C. Aspartic acid synthesis of crystalline gold nanoplates, nanoribbons, and nanowires in aqueous solutions. *J. Phys. Chem. C* **2008**, *112*, 5463.
(30) Mann, S. Life as a nanoscale phenomenon. *Angew. Chem., Int. Ed.* **2008**, *47*, 5306.
(31) Yang, D. P.; Chen, S. H.; Huang, P.; Wang, X. S.; Jiang, W. Q.; Pandoli, O.; Cui, D. X. Bacteria-template synthesized silver microspheres with hollow and porous structures as excellent SERS substrate. *Green Chem.* **2010**, *12*, 2038.
(32) Hall, S. R.; Shenton, W.; Engelhardt, H.; Mann, S. Site-specific organization of gold nanoparticles by biomolecular templating. *ChemPhysChem* **2001**, *2*, 184.
(33) Allred, D. B.; Sarikaya, M.; Baneyx, F.; Schwartz, D. T. Bacterial surface-layer proteins for electrochemical nanofabrication. *Electrochim. Acta* **2007**, *53*, 193.
(34) Puranik, S. S.; Joshi, H. M.; Ogale, S. B.; Paknikar, K. M. Hydrazine based facile synthesis and ordered assembly of metal nanoparticles (Au, Ag) on a bacterial surface layer protein template. *J. Nanosci. Nanotechnol.* **2008**, *8*, 3565.
(35) Garg, N.; Scholl, C.; Mohanty, A.; Jin, R. C. The role of bromide ions in seeding growth of Au nanorods. *Langmuir* **2010**, *26*, 10271.
(36) Li, L. M.; Weng, J. Enzymatic synthesis of gold nanoflowers with trypsin. *Nanotechnology* **2010**, *21*, 305603.
(37) Lin, Z.; Ye, Y.; Li, Q.; Xu, Z.; Wang, M. A further insight into the biosorption mechanism of Au(III) by infrared spectrometry. *BMC Biotechnol.* **2011**, *11*, 98.
(38) Weaver, S.; Taylor, D.; Gale, W.; Mills, G. Photoinitiated reversible formation of small gold crystallites in polymer gels. *Langmuir* **1996**, *12*, 4618.
(39) Wang, M. H.; Hu, J. W.; Li, Y. J.; Yeung, E. S. Au nanoparticle monolayers: preparation, structural conversion and their surface-enhanced Raman scattering effects. *Nanotechnology* **2010**, *21*, 145608.
(40) Hildebrandt, P.; Stockburger, M. Surface-enhanced resonance Raman spectroscopy of Rhodamine 6G adsorbed on colloidal silver. *J. Phys. Chem.* **1984**, *88*, 5935.
(41) Jiang, Y. Y.; Wu, X. J.; Li, Q.; Li, J. J.; Xu, D. S. Facile synthesis of gold nanoflowers with high surface-enhanced Raman scattering activity. *Nanotechnology* **2011**, *22*, 385601.